

Variable Switching Point Predictive Current Control of Quasi-Z-Source Inverters

Ayman Ayad^{*}, Petros Karamanakos[†], and Ralph Kennel^{*}

^{*} Chair of Electrical Drive Systems and Power Electronics, Technische Universität München, Munich, Germany

[†] Department of Electrical Engineering, Tampere University of Technology, Tampere, Finland

Email: ayman.francees@tum.de, p.karamanakos@ieee.org, ralph.kennel@tum.de

Abstract—This paper presents a variable switching point predictive current control (VSP²CC) for the quasi-Z-source inverter (qZSI). The proposed VSP²CC aims to regulate the current on the ac side as well as the inductor current and capacitor voltage of the quasi-Z-source network. Unlike the previously presented model predictive control (MPC) strategies for the qZSI, with the proposed control scheme the optimal switch position can be changed at any time instant within the sampling interval. By doing so, the shoot-through state can be applied for a shorter time than the sampling interval which in turn results in lower output and inductor currents ripples. Experimental results, based on an FPGA, are provided to verify the proposed control technique. As it is shown, in comparison with the conventional MPC, the proposed method results in lower inductor current ripples and less output current THD.

I. INTRODUCTION

Z-source inverter (ZSI) has been recently proposed as an effective alternative to the conventional voltage source inverter (VSI) [1]. The ZSI utilizes an impedance network, consisting of two identical inductors and two identical capacitors, and it includes an additional shoot-through state (at least one of the inverter legs is short-circuited) in order to boost the input dc voltage to the desired dc-link level [2], [3]. In this respect, the shoot-through problem is positively utilized, thus, the employed dead-time with the conventional inverters is not required. This in turn results in low output current/voltage distortion and high inverter reliability [4].

Thereafter, the quasi-Z-source inverter (qZSI) was introduced as an improved version of the classical ZSI [5]. Due to its extra advantages, such as continuous input current, smaller passive components, and common ground point between the input and the dc-link bus, the qZSI has been used in a wide range of applications, see [6]–[11].

The qZSI has been considered as a buck-boost converter that operates as both dc-dc and dc-ac converters in one single-stage. Consequently, it needs two decoupled controllers. The dc-side controller adjusts the capacitor voltage (dc-link voltage) by controlling the shoot-through duty cycle, while the ac-side controller manipulates the inverter modulation index to regulate the output ac current/voltage. The design of the conventional proportional-integral (PI) controllers for the qZSI has been examined and discussed in many works, see e.g. [8], [9], [12]–[14]. It has been shown that the PI control results in satisfactory performance; however, the design process is still

cumbersome since cascaded control loops are required for both sides of the converter [15].

As an alternative, *direct* model predictive control (MPC), also referred to as finite control set MPC (FCS-MPC), has been recently applied to the qZSI [15]–[19]. Thanks to its fast dynamic response, implementation simplicity, and ability to handle multiple control objectives [20]–[22], MPC has proved to be an effective control algorithm for the qZSI. In this strategy, based on the control objectives (the regulation of the output current, inductor current, and capacitor voltage to their reference values as well as control of the switching frequency), an optimization problem is formulated and solved to find the optimal control action (switch position). However, the solution to the optimization problem underlying MPC is applied for at least one sampling interval. This implies that the shoot-through state can be applied for more than one sampling interval. Consequently, when the converter operates at low switching frequency, the shoot-through state is applied for a long time. This leads to high inductor current ripples and output current total harmonic distortion (THD) [17].

Recently, some techniques have been proposed that include a “modulator” to the MPC scheme, with a goal to reduce the ripples of the variables of interest (e.g. current, torque, flux, etc.) [23]–[28]. This is done by formulating an optimization problem, the solution to which is the time instant within the sampling interval where the switches of the converter should change state in order for the ripples of concern to be minimized. As a result, the switching states that could lead to high ripples are applied for less time than with conventional MPC, resulting in an overall improved system performance.

Motivated by the advantages of the aforementioned approaches, this paper proposes a variable switching point predictive current control (VSP²CC) for the qZSI. In addition to the above-mentioned control objectives, the proposed scheme aims to reduce the output and inductor currents ripples by changing the switch position at any point within the sampling interval, thus, reducing the time the shoot-through state is applied. The performance of the proposed scheme is experimentally investigated based on a field programmable gate array (FPGA) Cyclone III-EP3C40Q240C8. The proposed method results in lower inductor current ripples and output current THD compared to the conventional MPC when operating the

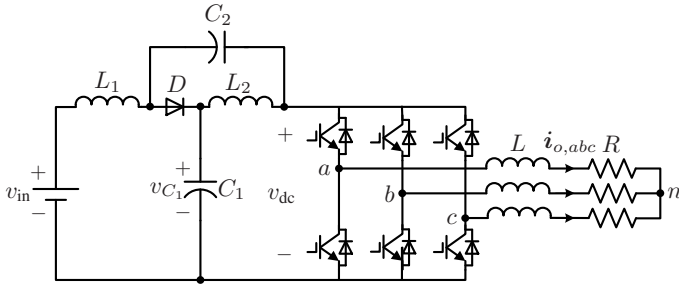
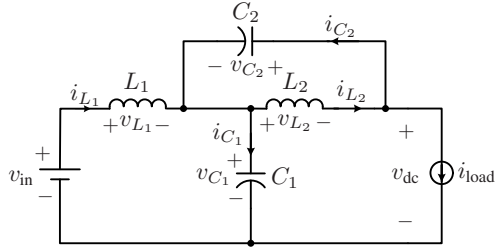
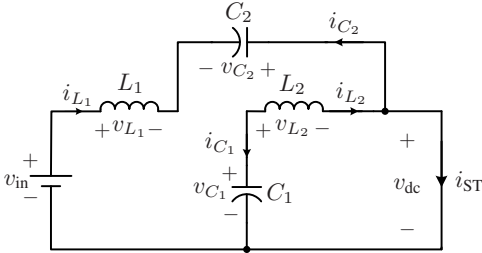


Fig. 1: Topology of the quasi-Z-source inverter (qZSI).



(a) Non-shoot-through state.



(b) Shoot-through state.

Fig. 2: Operation states of the qZSI.

converter at the same switching frequency.

This paper is structured as follows. Section II introduces the mathematical model of the qZSI. The proposed VSP²CC strategy is presented in Section III. In Section IV, experimental results are provided and discussed. Finally, the conclusion is drawn in Section V.

II. SYSTEM PHYSICAL MODEL

The system under discussion, consisting of a quasi-Z-source (qZS) network, a two-level three-phase inverter, and an RL load, is shown in Fig. 1. Depending on the operating state, the qZSI operates in two different states; shoot-through state and non-shoot-through state (comprising of the six active and two zero states of the conventional two-level voltage source inverter) as displayed in Fig. 2. Consequently, the physical model of the qZSI will be separately derived for each operating state. Then, the overall model of the system will be obtained.

Note that to reduce the computations, the output current is expressed in the stationary orthogonal system ($\alpha\beta$) instead of

the three-phase system (abc), i.e. $i_{o,\alpha\beta} = \mathbf{K}i_{o,abc}$ ¹ where \mathbf{K} is the Clarke transformation matrix

$$\mathbf{K} = \frac{2}{3} \begin{bmatrix} 1 & -\frac{1}{2} & -\frac{1}{2} \\ 0 & \frac{\sqrt{3}}{2} & -\frac{\sqrt{3}}{2} \end{bmatrix}. \quad (1)$$

The state vector includes the output current, the inductor currents, and the capacitor voltages, i.e. $\mathbf{x} = [i_{o,\alpha} \ i_{o,\beta} \ i_{L1} \ i_{L2} \ v_{C1} \ v_{C2}]^T \in \mathbb{R}^6$. The output and the inductor currents as well as the capacitor voltage compose the output vector², i.e. $\mathbf{y} = [i_{o,\alpha} \ i_{o,\beta} \ i_{L1} \ v_{C1}]^T \in \mathbb{R}^4$. Moreover, the system input is the three-phase switch positions $\mathbf{u}_{abc} \in \mathcal{U}^3$, where $\mathbf{u}_{abc} = [u_a \ u_b \ u_c]^T$ and $\mathcal{U} = \{0, 1\}$. Finally, the input dc voltage is considered as a disturbance to the system, i.e. $\mathbf{w} = v_{in} \in \mathbb{R}$.

A. Non-Shoot-Through State

During the non-shoot-through state, as shown in Fig. 2(a), the input voltage source and the inductors charge the capacitors and feed the load. Accordingly, the converter model is obtained by

$$\frac{d\mathbf{x}(t)}{dt} = \mathbf{F}_1\mathbf{x}(t) + \mathbf{G}_1\mathbf{u}_{abc}(t) + \mathbf{H}\mathbf{w}(t) \quad (2a)$$

$$\mathbf{y}(t) = \mathbf{E}\mathbf{x}(t), \quad (2b)$$

where³

$$\mathbf{F}_1 = \begin{bmatrix} -\frac{R}{L} & 0 & 0 & 0 & 0 & 0 \\ 0 & -\frac{R}{L} & 0 & 0 & 0 & 0 \\ 0 & 0 & 0 & 0 & -\frac{1}{L_1} & 0 \\ 0 & 0 & 0 & 0 & 0 & -\frac{1}{L_2} \\ -\frac{\mathbf{u}_{abc}^T \mathbf{K}^{-1}}{C_1} & -\frac{\mathbf{u}_{abc}^T \mathbf{K}^{-1}}{C_2} & \frac{1}{C_1} & 0 & 0 & 0 \\ -\frac{\mathbf{u}_{abc}^T \mathbf{K}^{-1}}{C_2} & -\frac{\mathbf{u}_{abc}^T \mathbf{K}^{-1}}{C_1} & 0 & \frac{1}{C_2} & 0 & 0 \end{bmatrix}$$

$$\mathbf{G}_1 = \hat{v}_{dc} \begin{bmatrix} \frac{1}{L} & 0 \\ 0 & \frac{1}{L} \\ 0 & 0 \\ 0 & 0 \\ 0 & 0 \\ 0 & 0 \end{bmatrix} \mathbf{K}, \quad \mathbf{H} = \begin{bmatrix} 0 \\ 0 \\ \frac{1}{L_1} \\ 0 \\ 0 \\ 0 \end{bmatrix},$$

$$\mathbf{E} = \begin{bmatrix} 1 & 0 & 0 & 0 & 0 & 0 \\ 0 & 1 & 0 & 0 & 0 & 0 \\ 0 & 0 & 1 & 0 & 0 & 0 \\ 0 & 0 & 0 & 0 & 1 & 0 \end{bmatrix}.$$

where R (L) is the load resistance (inductance), and \hat{v}_{dc} is the peak dc-link voltage, see the appendix.

¹Note that the subscript for vectors in the $\alpha\beta$ plane is dropped to simplify the notation. Vectors in the abc plane are denoted with the corresponding subscript.

²Due to the symmetry of the quasi-Z-source network, only one inductor current and one capacitor voltage are considered as output variables.

³For a matrix \mathbf{M} , $\mathbf{M}_{(:,i)}$ denotes its i th column.

B. Shoot-Through State

As shown in Fig. 2(b), at the shoot-through state, the diode is off and the load is short-circuited. During this state, the input voltage source and the capacitors charge the inductors. Consequently, the model is given by

$$\frac{d\mathbf{x}(t)}{dt} = \mathbf{F}_2\mathbf{x}(t) + \mathbf{G}_2\mathbf{u}_{abc}(t) + \mathbf{H}\mathbf{w}(t) \quad (3a)$$

$$\mathbf{y}(t) = \mathbf{E}\mathbf{x}(t), \quad (3b)$$

where

$$\mathbf{F}_2 = \begin{bmatrix} -\frac{R}{L} & 0 & 0 & 0 & 0 & 0 \\ 0 & -\frac{R}{L} & 0 & 0 & 0 & 0 \\ 0 & 0 & 0 & 0 & 0 & \frac{1}{L_1} \\ 0 & 0 & 0 & 0 & \frac{1}{L_2} & 0 \\ 0 & 0 & 0 & -\frac{1}{C_1} & 0 & 0 \\ 0 & 0 & -\frac{1}{C_2} & 0 & 0 & 0 \end{bmatrix},$$

and \mathbf{G}_2 is the zero matrix of appropriate dimensions.

C. Continuous-Time Model

The derived models (2) and (3) can compose one model that precisely describes the different operating states of the qZSI. To do so, an auxiliary binary variable d_{aux} is introduced. This variable indicates the state at which the converter operates, i.e.

$$d_{aux} = \begin{cases} 0 & \text{if non-shoot-through state (active or zero state)} \\ 1 & \text{if shoot-through state} \end{cases} \quad (4)$$

The transition from non-shoot-through state to shoot-through state, and vice versa, is input-dependent, thus (4) can be written as

$$d_{aux} = \begin{cases} 0 & \text{if } u_x \neq \bar{u}_x \forall x \in \{a, b, c\} \\ 1 & \text{if } \exists x \in \{a, b, c\} \text{ s.t. } u_x = \bar{u}_x = 1 \end{cases} \quad (5)$$

Taking all the above into account, the model of the converter can be written as

$$\frac{d\mathbf{x}(t)}{dt} = \mathbf{F}\mathbf{x}(t) + \mathbf{G}\mathbf{u}_{abc}(t) + \mathbf{H}\mathbf{w}(t) \quad (6a)$$

$$\mathbf{y}(t) = \mathbf{E}\mathbf{x}(t), \quad (6b)$$

where

$$\mathbf{F} = \begin{bmatrix} -\frac{R}{L} & 0 & 0 & 0 & 0 & 0 \\ 0 & -\frac{R}{L} & 0 & 0 & 0 & 0 \\ 0 & 0 & 0 & 0 & \frac{d_{aux}-1}{L_1} & \frac{d_{aux}}{L_1} \\ 0 & 0 & 0 & 0 & \frac{d_{aux}}{L_2} & \frac{d_{aux}-1}{L_2} \\ \frac{m_1}{C_1} & \frac{m_2}{C_1} & \frac{1-d_{aux}}{C_1} & -\frac{d_{aux}}{C_1} & 0 & 0 \\ \frac{m_1}{C_2} & \frac{m_2}{C_2} & -\frac{d_{aux}}{C_2} & \frac{1-d_{aux}}{C_2} & 0 & 0 \end{bmatrix}$$

and

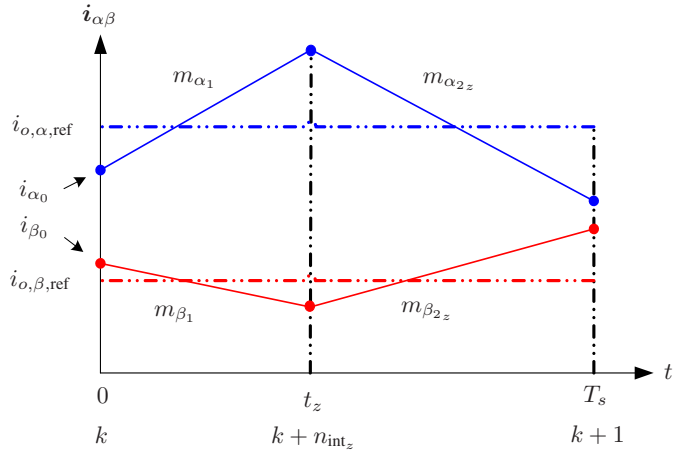


Fig. 3: Variable switching point concept.

$$m_1 = (d_{aux} - 1)\mathbf{u}_{abc}^T \mathbf{K}_{(:,1)}^{-1}, \quad m_2 = (d_{aux} - 1)\mathbf{u}_{abc}^T \mathbf{K}_{(:,2)}^{-1}$$

Moreover, $\mathbf{G} = (1 - d_{aux})\mathbf{G}_1$.

D. Discrete-Time Model

To compute the predictions of the variables of interest, the discrete-time model of the qZSI is required. Hence, by using forward Euler approximation, the continuous-time model (6) is discretized as follows

$$\mathbf{x}(k+1) = \mathbf{A}\mathbf{x}(k) + \mathbf{B}\mathbf{u}_{abc}(k) + \mathbf{D}\mathbf{w}(k) \quad (7a)$$

$$\mathbf{y}(k) = \mathbf{C}\mathbf{x}(k), \quad (7b)$$

where $\mathbf{A} = (\mathbf{F} + \mathbf{I})T_s$, $\mathbf{B} = \mathbf{G}T_s$, $\mathbf{D} = \mathbf{H}T_s$ and $\mathbf{C} = \mathbf{E}$. Moreover, \mathbf{I} is the identity matrix of appropriate dimensions, T_s denotes the sampling interval, and $k \in \mathbb{N}$.

III. VARIABLE SWITCHING POINT PREDICTIVE CURRENT CONTROL STRATEGY

A. Control Objective

The main objective of the proposed VSP²CC strategy is to regulate the output current, inductor current, and capacitor voltage along their reference values. In addition, the switching frequency is to be kept relatively low in order to reduce the switching losses. Moreover, the output current ripples are to be minimized. To achieve these goals, the control algorithm calculates the variable switching point (VSP) at which the optimal switch position should be applied. The VSP is calculated such that the squared rms current error of the output current is minimized.

B. Proposed Control Algorithm

As mentioned, the VSP t_z , i.e. $t_z \in [0, T_s)$ is calculated based on the minimization of the squared rms error of the output current, where $t_z = n_{int_z}^{(k)} T_s$, with $n_{int_z}^{(k)} \in [0, 1)$ being the normalized time instant between the time-steps k and $k+1$. Fig. 3 shows the main concept of VSP where the slopes of

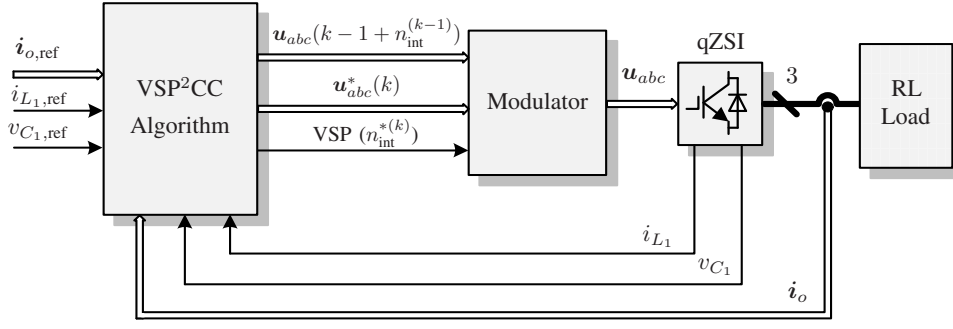


Fig. 4: Variable switching point predictive current control for the qZSI.

both α and β currents are assumed to be constant over one sampling interval. Accordingly, the squared rms current error (e_{rms^2}) is given by

$$e_{rms^2} = \frac{1}{T_s} \left(\int_0^{t_z} (\mathbf{i}_{\alpha\beta,ref} - \mathbf{i}_{\alpha\beta}(t, \mathbf{u}_{abc}(k)))^2 dt + \int_{t_z}^{T_s} (\mathbf{i}_{\alpha\beta,ref} - \mathbf{i}_{\alpha\beta}(t, \mathbf{u}_{abc}(k + n_{int_z}^{(k)})))^2 dt \right), \quad (8)$$

where $\mathbf{i}_{\alpha\beta,ref}$ is the $\alpha\beta$ current reference. Moreover, $\mathbf{i}_{\alpha\beta}(t, \mathbf{u}_{abc}(k))$ and $\mathbf{i}_{\alpha\beta}(t, \mathbf{u}_{abc}(k + n_{int_z}^{(k)}))$ are the output currents resulting from the applied switch position and candidate switch positions, respectively, with $z \in \{1, 2, \dots, 8\}$ denoting the corresponding switch position. Note that Fig. 3 shows the current slopes resulting from the applied switch position (i.e. $m_{\alpha_1}, m_{\beta_1}$) and only one of the candidate switch positions (i.e. $m_{\alpha_{2z}}, m_{\beta_{2z}}$).

In order to minimize (8) its derivative is set equal to zero. This yields

$$t_z = \frac{(2\mathbf{i}_{\alpha\beta_0} - 2\mathbf{i}_{\alpha\beta,ref} + T_s \mathbf{m}_{\alpha\beta_{2z}})(\mathbf{m}_{\alpha\beta_{2z}} - \mathbf{m}_{\alpha\beta_1})}{(2\mathbf{m}_{\alpha\beta_1} - \mathbf{m}_{\alpha\beta_{2z}})(\mathbf{m}_{\alpha\beta_1} - \mathbf{m}_{\alpha\beta_{2z}})} \quad (9)$$

where $\mathbf{i}_{\alpha\beta_0}$ denotes the measured $\alpha\beta$ currents at time-step k (see Fig. 3). In addition, $\mathbf{m}_{\alpha\beta_1} = [m_{\alpha_1} \ m_{\beta_1}]^T$ and $\mathbf{m}_{\alpha\beta_{2z}} = [m_{\alpha_{2z}} \ m_{\beta_{2z}}]^T$.

The following algorithm, executed at time-step k , is used to calculate the VSP with the corresponding optimal switch position.

Step 1: First, it is assumed that the switch position $\mathbf{u}_{abc}(k-1 + n_{int}^{(k-1)})$ applied at time instant $(k-1 + n_{int}^{(k-1)})T_s$ is also applied at time-step k . Then, by using the system model (7) and the measured output current, the predicted output current at step $k+1$ ($\mathbf{i}_{\alpha\beta}(k+1)$) is computed. Hence, the first current slopes can be given by

$$\mathbf{m}_{\alpha\beta_1} = \frac{\mathbf{i}_{\alpha\beta}(k+1) - \mathbf{i}_{\alpha\beta}(k)}{T_s}. \quad (10)$$

Step 2: Then, the predicted output current is recomputed assuming that the switch position at time-step k , i.e. $\mathbf{u}_{abc}(k)$,

can be any one of the eight possibilities (six active switch positions, one zero switch position, and one shoot-through switch position). Then, the possible current slopes are calculated as

$$\mathbf{m}_{\alpha\beta_{2z}} = \frac{\mathbf{i}_{\alpha\beta_z}(k+1) - \mathbf{i}_{\alpha\beta}(k)}{T_s}. \quad (11)$$

Using the current slopes in (10) and (11), the VSP (9) can be calculated.

Step 3: Based on the computed VSP, the predictions of the state and output variables are computed at two different time instances. The first predictions are computed at $k + n_{int_z}^{(k)}$, where t_z is used instead of T_s in (7). For the second set of predictions at $k+1$, the time interval $(T_s - t_z)$ is used.

Step 4: Next, a cost function is formulated as follows

$$J(k) = \sum_{\xi \in \mathcal{S}} \left(\|\mathbf{y}_{ref} - \mathbf{y}(k + \xi|k)\|_{\mathbf{Q}}^2 \right) + \lambda_u \|\Delta \mathbf{u}_{abc}(k|k)\|_2^2, \quad (12)$$

with $\mathcal{S} = \{n_{int}, 1\}$ and $\mathbf{y}_{ref} = [i_{o,\alpha,ref} \ i_{o,\beta,ref} \ i_{L1,ref} \ v_{C1,ref}]^T$. The second term is added to adjust the switching frequency of the converter, where $\Delta \mathbf{u}_{abc}(k) = \mathbf{u}_{abc}(k) - \mathbf{u}_{abc}(k-1)$. Moreover, the weighting factor λ_u and the diagonal positive semidefinite weighting matrix⁴ $\mathbf{Q} \in \mathbb{R}^{4 \times 4}$ are added to set the trade-off between the tracking performance and the converter switching frequency.

Then, in order to find the optimal switch position and the corresponding VSP, the following optimization problem is solved in real time

$$\begin{aligned} & \text{minimize} && J(k) \\ & \mathbf{u}_{abc} && \\ & \text{subject to} && \text{eq. (7)}. \end{aligned} \quad (13)$$

This yields the pair $\mathbf{U}^*(k) = \{\mathbf{u}_{abc}^*(k + n_{int}), n_{int}^{*(k)}\}$.

Finally, a modulator is used to apply the final switching signals to the converter. The modulator is working on a higher sampling frequency than the one of the MPC algorithm itself.

⁴The squared norm weighted with the positive (semi)definite matrix \mathbf{W} is given by $\|\xi\|_{\mathbf{W}}^2 = \xi^T \mathbf{W} \xi$.

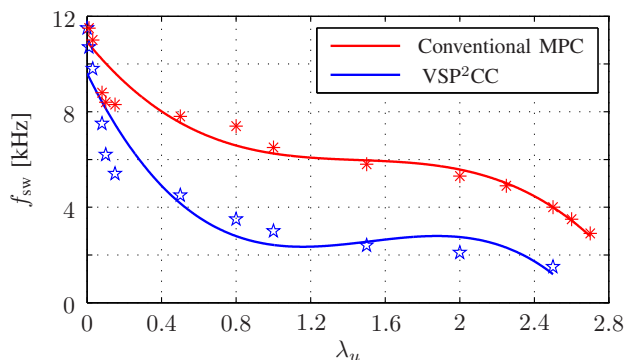


Fig. 5: The effect of the weighting factor (λ_u) on the switching frequency for both conventional MPC and VSP²CC.

The modulator first outputs the previously applied switch position $\mathbf{u}_{abc}(k-1 + n_{\text{int}}^{(k-1)})$ until time instant t_z . Subsequently, it applies the new optimal switch position $\mathbf{u}_{abc}^*(kn_{\text{int}})$ until the end of the sampling interval. At the next time-step $k+1$, the control procedure is repeated with new measurements. The block diagram of VSP²CC for the qZSI is shown in Fig. 4.

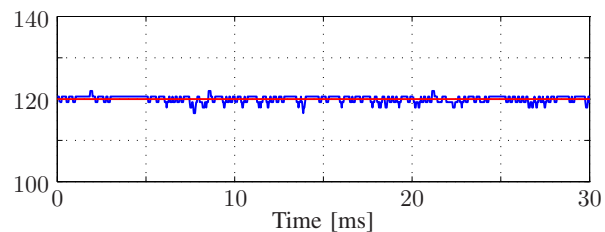
IV. EXPERIMENTAL RESULTS

To examine the performance of the proposed VSP²CC strategy for the qZSI configuration, shown in Fig. 1, experiments were conducted in the laboratory. For the sake of comparison, the conventional MPC is also investigated [16]. Both control algorithms are implemented on a low-cost, low-power field programmable logic array (FPGA) Cyclone III-EP3C40Q240C8, with 39,600 logic elements, 126 multipliers, and 1,161,216 total RAM bits.

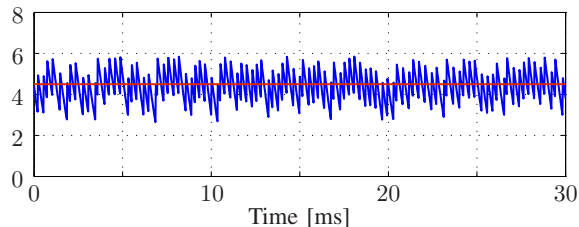
To compensate for the time delay introduced by the proposed and conventional algorithm, a delay compensation strategy is applied [29]. Concerning the computational demand, VSP²CC needs higher calculation time than the conventional MPC. For instance, the conventional MPC algorithms is executed in $3\mu\text{s}$, while the proposed VSP²CC requires $5\mu\text{s}$. By using an FPGA, both algorithms can be easily implemented.

The system parameters are $v_{\text{in}} = 70\text{ V}$, $L_1 = L_2 = 1\text{ mH}$, $C_1 = C_2 = 480\mu\text{F}$, $R = 10\Omega$, and $L = 10\text{ mH}$. According to the desired output power ($P_{o,\text{ref}} = 315\text{ W}$), the output current reference $i_{o,\text{ref}}$ is set to 4 A , while the inductor current reference is equal to 4.5 A ($i_{L_1,\text{ref}} = P_{o,\text{ref}}/v_{\text{in}}$). In order to keep the peak dc-link voltage \hat{v}_{dc} at 180 V , the capacitor voltage reference $v_{C_1,\text{ref}}$ is set to 120 V , see the steady-state analysis in the appendix. The sampling interval used for the VSP²CC algorithm is $T_s = 25\mu\text{s}$, while it is $T_{s_m} = 0.25\mu\text{s}$ for the modulator block.

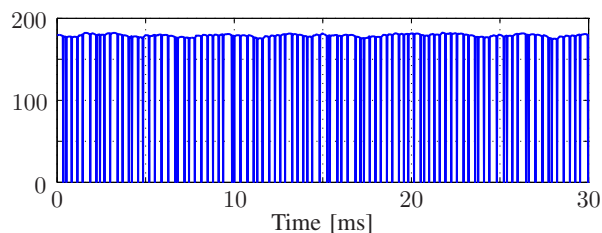
Furthermore, the converter operates at the desired switching frequency f_{sw} , by adjusting Q and λ_u in (12). Fig. 5 shows how the weighting factor λ_u affects the operating switching frequency of the converter with both the conventional MPC and proposed VSP²CC schemes.



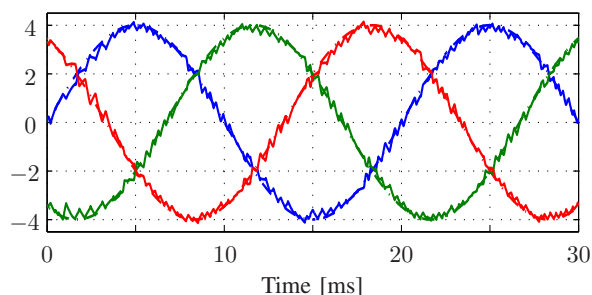
(a) Capacitor voltage v_{C_1} and its reference in [V].



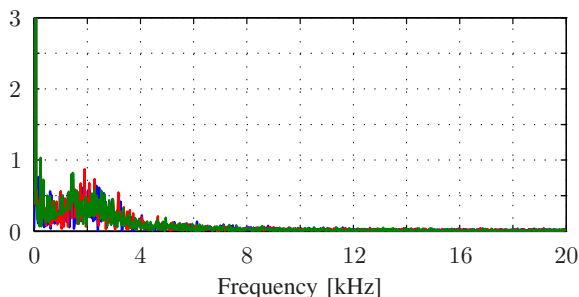
(b) Inductor current i_{L_1} and its reference in [A].



(c) Dc-link voltage v_{dc} in [V].

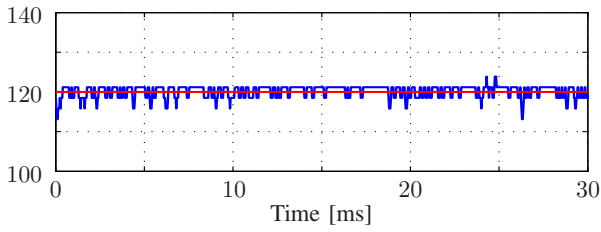


(d) Three-phase output current i_o (solid lines) and their references (dash-dotted lines) in [A].

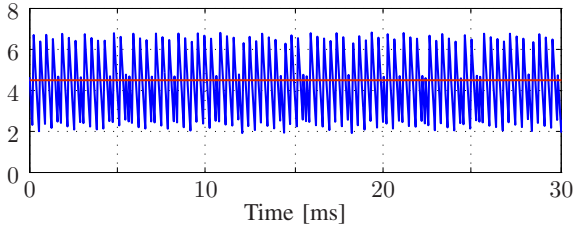


(e) Output current spectrum (%), THD = 4.21 %.

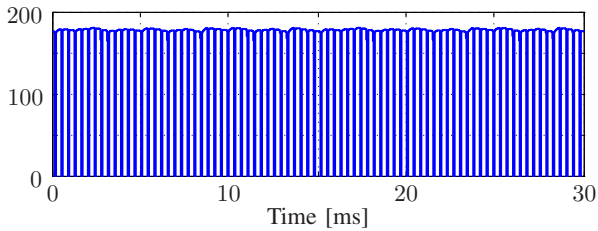
Fig. 6: Experimental results of the dc and ac side of the qZSI with the VSP²CC. The sampling interval is $T_s = 25\mu\text{s}$ and the switching frequency is $f_{\text{sw}} \approx 3.4\text{ kHz}$.



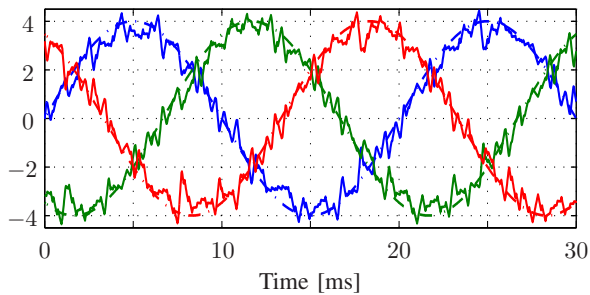
(a) Capacitor voltage v_{C_1} and its reference in [V].



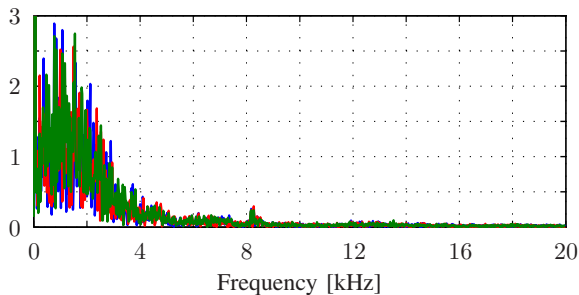
(b) Inductor current i_{L_1} and its reference in [A].



(c) Dc-link voltage v_{dc} in [V].



(d) Three-phase output current i_o (solid lines) and their references (dash-dotted lines) in [A].



(e) Output current spectrum (%), THD = 12.49%.

Fig. 7: Experimental results of the dc and ac side of the qZSI with the conventional MPC. The sampling interval is $T_s = 25 \mu\text{s}$ and the switching frequency is $f_{sw} \approx 3.4 \text{ kHz}$.

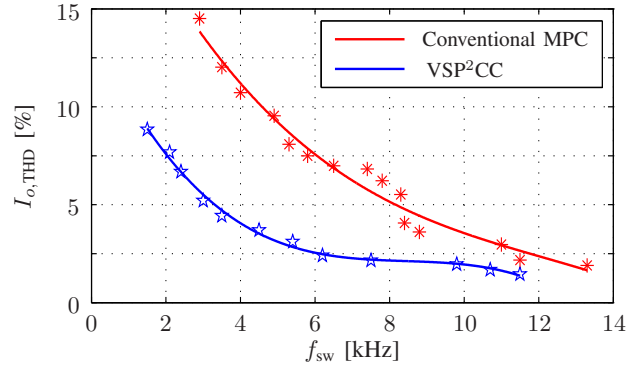


Fig. 8: Trade-off between the current THD $I_{o,THD}$ and the switching frequency f_{sw} for the VSP²CC and conventional MPC.

A. Steady-State Operation

The steady-state response of the qZSI is examined with the proposed VSP²CC and the conventional MPC. The operating average switching frequency is adjusted to $f_{sw} \approx 3.4 \text{ kHz}$ for both controllers by setting λ_u in (12) as 0.75 and 2.6 with VSP²CC and conventional MPC, respectively.

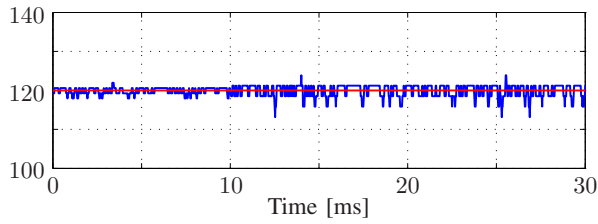
The experimental results for VSP²CC and conventional MPC are shown in Figs. 6 and 7, respectively. As can be seen, the dc-side variables effectively track their reference values in both examined cases. The capacitor voltages (Figs. 6(a) and 7(a)) and the inductor currents (Figs. 6(b) and 7(b)) are regulated along their reference values resulting in the desired peak dc-link voltage of 180 V (Figs. 6(c) and 7(c)). Although both controllers introduce zero steady-state error for both dc quantities, VSP²CC produces inductor current of about 50% less ripple than the conventional MPC.

As for the ac side, Figs. 6(d) and 7(d) show that the output current accurately tracks its reference with both VSP²CC and conventional MPC. However, VSP²CC produces output current THD of 4.21%, notably lower than the THD with the conventional MPC (12.49%), see Figs. 6(e) and 7(e).

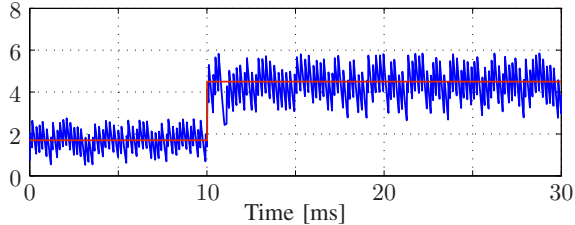
Furthermore, the trade-off between the output current THD and the switching frequency of the proposed VSP²CC and the conventional MPC is investigated. In this experiment, λ_u is appropriately tuned to obtain a wide range of switching frequencies. The results are approximated by a third degree polynomial and shown in Fig. 8. As can be observed, the VSP²CC introduces lower THD values than the conventional MPC over the whole range of the switching frequencies.

B. Transient Response

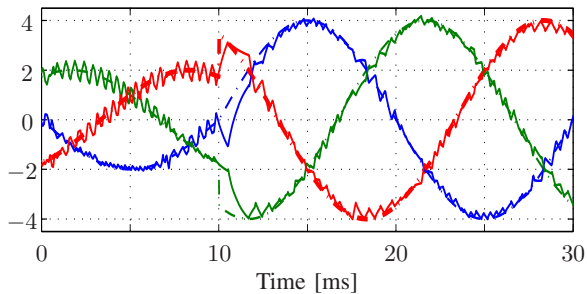
The transient behavior of the proposed VSP²CC and conventional MPC are scrutinized under a step change in the output current reference. The output current is stepped up from 2 A to 4 A. Consequently, the inductor current reference is changed from 1.7 A to 4.5 A, while the capacitor voltage reference is kept fixed at 120 V.



(a) Capacitor voltage v_{C_1} and its reference in [V].

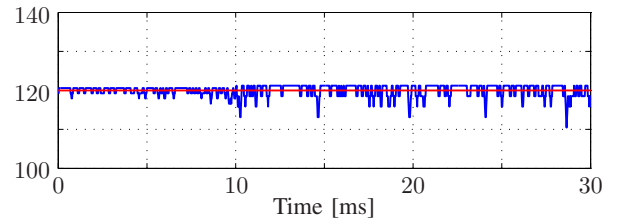


(b) Inductor current i_{L_1} and its reference in [A].

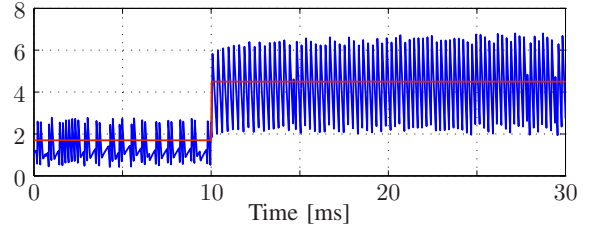


(c) Three-phase output current i_o (solid lines) and their references (dash-dotted lines) in [A].

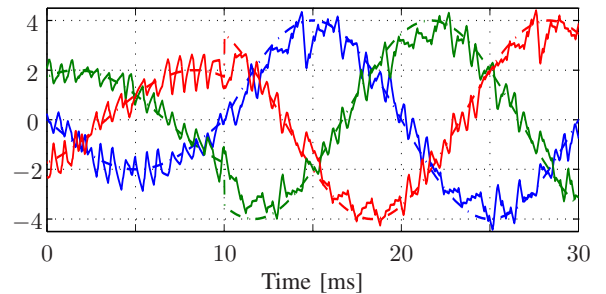
Fig. 9: Experimental results of the dc and ac side of the qZSI with VSP²CC under a step-up change in the output current reference.



(a) Capacitor voltage v_{C_1} and its reference in [V].



(b) Inductor current i_{L_1} and its reference in [A].



(c) Three-phase output current i_o (solid lines) and their references (dash-dotted lines) in [A].

Fig. 10: Experimental results of the dc and ac side of the qZSI with conventional MPC under a step-up change in the output current reference.

The dc- and ac-side results are shown in Figs. 9 and 10 for VSP²CC and conventional MPC, respectively. With both control schemes, the capacitor voltages are well regulated along their reference values, see Figs. 9(a) and 10(a). Additionally, as can be seen in Figs. 9(b) and 10(b), the inductor currents track their references both before and after the step change. Although both control schemes introduce very fast transient response, VSP²CC shows lower current ripples at both operating points.

As for the ac side, the proposed VSP²CC and conventional MPC achieve zero steady-state error (Figs. 9(c) and 10(c)) with very short transient time. It is also clear that VSP²CC delivers lower output current distortion. This verifies the theory that if the shoot-through state is applied for less time than the sampling interval, the inductor and output current ripples (as quantified by the output current THD) can be significantly reduced. As a result, the performance of the converter can be considerably improved.

V. CONCLUSIONS

This paper presents a variable switching point predictive current control (VSP²CC) for the quasi-Z-source inverter

(qZSI). The proposed algorithm controls both sides of the converter, i.e. the output current on the ac side as well as the inductor current and capacitor voltage on the dc side. In order to improve the system behavior, VSP²CC changes the (optimal) state of the switches at that time instant that results in minimal inductor and output current ripples. By doing so, the switch position that results in high current ripples (i.e. the shoot-through state) is applied for a shorter time. The performance of the proposed method and conventional MPC are experimentally investigated based on an FPGA. Although the proposed algorithm requires higher calculation time than the conventional MPC, by using high performance and high optimized FPGA the implementation of the proposed algorithm is possible. It is shown that the proposed strategy results in lower inductor current ripples and less output current THD compared with the conventional scheme when the converter operates at the same switching frequency.

APPENDIX

At steady-state operation, and according to the inductor volt-second balance, the average voltage of the inductors is zero over one time window $T_1 = n_1 T_s$, with $n_1 \in \mathbb{N}^+$. Note that

$T_1 \approx 1/f_{sw}$, with f_{sw} being the *average* switching frequency⁵. Therefore, the voltages of the capacitors C_1 and C_2 , v_{C_1} and v_{C_2} , respectively, as well as the currents i_{L_1} and i_{L_2} of the inductors L_1 and L_2 , respectively, are deduced as follows, assuming that $C_1 = C_2$ and $L_1 = L_2$

$$v_{C_1} = \frac{1-d}{1-2d}v_{in}, \quad v_{C_2} = \frac{d}{1-2d}v_{in}, \quad (14a)$$

$$i_{L_1} = i_{L_2} = \frac{1-d}{1-2d}i_{load}, \quad (14b)$$

where i_{load} is the load current as shown in Fig. 2(a). The *average* shoot-through duty cycle of the qZSI $d \in [0, 0.5)$ is defined as

$$d = \frac{T_0}{T_1} = \frac{n_0 T_s}{n_1 T_s} = \frac{n_0}{n_1}, \quad (15)$$

where T_0 is the time interval within the time window T_1 for which the load is short-circuited, i.e. the shoot-through time interval, and $n_0 < \frac{n_1}{2}$, $n_0 \in \mathbb{N}^+$. Moreover, the peak value of the dc-link voltage during the non-shoot-through period is

$$\hat{v}_{dc} = v_{C_1} + v_{C_2} = \frac{1}{1-2d}v_{in} \quad (16)$$

REFERENCES

- [1] Y. Siwakoti, F. Z. Peng, F. Blaabjerg, P. C. Loh, and G. Town, "Impedance-source networks for electric power conversion part I: A topological review," *IEEE Trans. Power Electron.*, vol. 30, no. 2, pp. 699–716, Feb. 2015.
- [2] F. Z. Peng, "Z-source inverter," *IEEE Trans. Ind. Appl.*, vol. 39, no. 2, pp. 504–510, 2003.
- [3] A. Ayad, M. Ismeil, R. Kennel, and M. Orabi, "Experimental studies on a single-phase improved switched inductor Z-source inverter," in *Proc. Eur. Power Electron. Conf.*, Lille, France, Sep. 2013, pp. 1–10.
- [4] Y. Liu, H. Abu-Rub, and B. Ge, "Z-source/quasi-Z-source inverters: Derived networks, modulations, controls, and emerging applications to photovoltaic conversion," *IEEE Ind. Electron. Mag.*, vol. 8, no. 4, pp. 32–44, Dec. 2014.
- [5] J. Anderson and F. Peng, "Four quasi-Z-source inverters," in *Proc. IEEE Power Electron. Spec. Conf.*, Rhodes, Greece, Jun. 2008, pp. 2743–2749.
- [6] F. Guo, L. X. Fu, C. H. Lin, C. Li, W. Choi, and J. Wang, "Development of an 85 kW bidirectional quasi-Z-source inverter with DC-link feed-forward compensation for electric vehicle applications," *IEEE Trans. Power Electron.*, vol. 28, no. 12, pp. 5477–5488, Dec. 2013.
- [7] J. Liu, S. Jiang, D. Cao, and F. Z. Peng, "A digital current control of quasi-Z-source inverter with battery," *IEEE Trans. Ind. Informat.*, vol. 9, no. 2, pp. 928–937, May 2013.
- [8] Y. Li, S. Jiang, J. Cintron-Rivera, and F. Z. Peng, "Modeling and control of quasi-Z-source inverter for distributed generation applications," *IEEE Trans. Ind. Electron.*, vol. 60, no. 4, pp. 1532–1541, Apr. 2013.
- [9] A. Ayad, S. Hanafiah, and R. Kennel, "A comparison of quasi-Z-source inverter and traditional two-stage inverter for photovoltaic application," in *Proc. Int. Expo. and Conf. Power Electron., Intelligent Motion, Renew. Energy Management*, Nuremberg, Germany, May 2015, pp. 1–8.
- [10] B. Ge, H. Abu-Rub, F. Z. Peng, Q. Lei, A. de Almeida, and F. Ferreira, "An energy-stored quasi-Z-source inverter for application to photovoltaic power system," *IEEE Trans. Ind. Electron.*, vol. 60, no. 10, pp. 4468–4481, Oct. 2013.
- [11] A. Battiston, E. H. Miliiani, S. Pierfederici, and F. Meibody-Tabar, "Efficiency improvement of a quasi-Z-source inverter-fed permanent-magnet synchronous machine-based electric vehicle," *IEEE Trans. Transport. Electrification*, vol. 2, no. 1, pp. 14–23, Mar. 2016.
- [12] Q. Lei, F. Z. Peng, and B. Ge, "Transient modeling of current-fed quasi-Z-source inverter," in *Proc. IEEE Energy Convers. Congr. Expo.*, Sep. 2011, pp. 2283–2287.
- [13] F. Guo, L. Fu, C. H. Lin, C. Li, and J. Wang, "Small signal modeling and controller design of a bidirectional quasi-Z-source inverter for electric vehicle applications," in *Proc. IEEE Energy Convers. Congr. Expo.*, Sep. 2012, pp. 2223–2228.
- [14] Y. Siwakoti, F. Z. Peng, F. Blaabjerg, P. C. Loh, and G. Town, "Impedance-source networks for electric power conversion part II: Review of control and modulation techniques," *IEEE Trans. Power Electron.*, vol. 30, no. 4, pp. 1887–1906, April. 2015.
- [15] A. Ayad, P. Karamanakos, and R. Kennel, "Direct model predictive current control strategy of quasi-Z-source inverters," *IEEE Trans. Power Electron.*, DOI: 10.1109/TPEL.2016.2610459, to appear.
- [16] A. Ayad and R. Kennel, "Direct model predictive control of quasi-Z-source inverter compared with the traditional PI-based PWM control," in *Proc. Eur. Power Electron. Conf.*, Geneva, Switzerland, Sep. 2015, pp. 1–9.
- [17] A. Ayad, P. Karamanakos, and R. Kennel, "Direct model predictive current control of quasi-Z-source inverters," in *Proc. IEEE Int. Symp. Pred. Control of Elect. Drives and Power Electron.*, Valparaíso, Chile, Oct. 2015, pp. 1–6.
- [18] A. Ayad, P. Karamanakos, and R. Kennel, "Direct model predictive voltage control of quasi-Z-source inverters with LC filters," in *Proc. Eur. Power Electron. Conf.*, Karlsruhe, Germany, Sep. 2016, to appear, pp. 1–10.
- [19] A. Ayad, P. Karamanakos, and R. Kennel, "Direct model predictive control with an extended prediction horizon for quasi-Z-source inverters," in *Proc. IEEE Ind. Electron. Society IECON*, Florence, Italy, Oct. 2016, to appear, pp. 1–6.
- [20] P. Cortés, M. P. Kazmierkowski, R. M. Kennel, D. E. Quevedo, and J. Rodríguez, "Predictive control in power electronics and drives," *IEEE Trans. Ind. Electron.*, vol. 55, no. 12, pp. 4312–4324, Dec. 2008.
- [21] P. Karamanakos, T. Geyer, N. Oikonomou, F. D. Kieferndorf, and S. Manias, "Direct model predictive control: A review of strategies that achieve long prediction intervals for power electronics," *IEEE Ind. Electron. Mag.*, vol. 8, no. 1, pp. 32–43, Mar. 2014.
- [22] S. Kouro, M. A. Perez, J. Rodríguez, A. M. Llor, and H. A. Young, "Model predictive control: MPC's role in the evolution of power electronics," *IEEE Ind. Electron. Mag.*, vol. 9, pp. 8–21, 2015.
- [23] P. Stolze, P. Karamanakos, M. Tomlinson, R. Kennel, T. Mouton, and S. Manias, "Heuristic variable switching point predictive current control for the three-level neutral point clamped inverter," in *Proc. IEEE Int. Symp. Pred. Control of Elect. Drives and Power Electron.*, Munich, Germany, Oct. 2013, pp. 1–8.
- [24] Y. Zhang, W. Xie, Z. Li, and Y. Zhang, "Model predictive direct power control of a PWM rectifier with duty cycle optimization," *IEEE Trans. Power Electron.*, vol. 28, no. 11, pp. 5343–5351, Nov. 2013.
- [25] P. Karamanakos, P. Stolze, R. M. Kennel, S. Manias, and H. du Toit Mouton, "Variable switching point predictive torque control of induction machines," *IEEE J. Emerg. Sel. Topics Power Electron.*, vol. 2, no. 2, pp. 285–295, Jun. 2014.
- [26] L. Tarisciotti, P. Zanchetta, A. Watson, S. Bifaretti, and J. C. Clare, "Modulated model predictive control for a seven-level cascaded H-bridge back-to-back converter," *IEEE Trans. Ind. Electron.*, vol. 61, no. 10, pp. 5375–5383, Oct. 2014.
- [27] P. Stolze, P. Karamanakos, R. Kennel, S. Manias, and C. Endisch, "Effective variable switching point predictive current control for ac low voltage drives," *Int. J. of Control*, vol. 88, no. 7, pp. 1366–1378, 2015.
- [28] I. Alevras, P. Karamanakos, S. Manias, and R. Kennel, "Variable switching point predictive torque control with extended prediction horizon," in *Proc. IEEE Int. Conf. on Ind. Tech. (ICIT)*, Seville, Spain, 2015, pp. 2352–2357.
- [29] P. Cortés, J. Rodríguez, C. Silva, and A. Flores, "Delay compensation in model predictive current control of a three-phase inverter," *IEEE Trans. Ind. Electron.*, vol. 59, no. 2, pp. 1323–1325, 2012.

⁵With MPC the switching frequency is variable and the *average* switching frequency is used to indicate the operating switching frequency of the converter.